

MILLIHERTZ QUASI-PERIODIC OSCILLATIONS AND THERMONUCLEAR BURSTS FROM TERZAN 5: A SHOWCASE OF BURNING REGIMES.

M. LINARES^{1,5}, D. ALTAMIRANO², D. CHAKRABARTY¹, A. CUMMING³, L. KEEK⁴

Published in The Astrophysical Journal on 2012 March 9, Volume 748, Issue 2.

ABSTRACT

We present a comprehensive study of the thermonuclear bursts and millihertz quasi-periodic oscillations (mHz QPOs) from the neutron star (NS) transient and 11 Hz X-ray pulsar IGR J17480–2446, located in the globular cluster Terzan 5. The increase in burst rate that we find during its 2010 outburst, when persistent luminosity rises from 0.1 to 0.5 times the Eddington limit, is in qualitative agreement with thermonuclear burning theory yet opposite to all previous observations of thermonuclear bursts. Thermonuclear bursts gradually evolved into a mHz QPO when the accretion rate increased, and vice versa. The mHz QPOs from IGR J17480–2446 resemble those previously observed in other accreting NSs, yet they feature lower frequencies (by a factor ~ 3) and occur when the persistent luminosity is higher (by a factor 4–25). We find four distinct bursting regimes and a steep (close to inverse cubic) decrease of the burst recurrence time with increasing persistent luminosity. We compare these findings to nuclear burning models and find evidence for a transition between the pure helium and mixed hydrogen/helium ignition regimes when the persistent luminosity was about 0.3 times the Eddington limit. We also point out important discrepancies between the observed bursts and theory, which predicts brighter and less frequent bursts, and suggest that an additional source of heat in the NS envelope is required to reconcile the observed and expected burst properties. We discuss the impact of NS magnetic field and spin on the expected nuclear burning regimes, in the context of this particular pulsar.

Subject headings: accretion, accretion disks — binaries: close — globular clusters: individual (Terzan 5) — stars: neutron — X-rays: binaries — X-rays: individual (IGR J17480–2446)

1. INTRODUCTION

Matter accreted onto neutron stars (NSs) is piled up and compressed, settling towards regions of increasing density and temperature. In this process, depending on the rate at which accretion proceeds, both stable and unstable thermonuclear burning of the accreted H and He into heavier elements are expected (Fujimoto et al. 1981). The main parameter thought to determine the different burning regimes is the mass accretion rate on the NS per unit surface area, \dot{m} (e.g. Fujimoto et al. 1981; Bildsten 1998). When the burning layer becomes thermally unstable heat cannot be transported as fast as it is produced and a thermonuclear runaway occurs, producing a shell flash that releases 10^{38} – 10^{39} erg in tens of seconds (we do not discuss herein long bursts and superbursts, which are more energetic, 10^{40} – 10^{42} erg, and much less common; e.g., Keek & in’t Zand 2008). Most of the energy is deposited in the outermost layers of the NS within a few seconds and radiated away thermally for tens of seconds while the photosphere cools down. Type I X-ray bursts, which feature the spectral imprint of such photospheric cooling, were discovered in low-mass X-ray binaries (LMXBs) more than

30 years ago (Grindlay et al. 1976; Belian et al. 1976; Hoffman et al. 1978) and promptly identified as thermonuclear bursts from accreting NSs (Woosley & Taam 1976; Maraschi & Cavaliere 1977; Lewin & Joss 1977). Joss & Li (1980) pointed out that a strong NS magnetic field can act to stabilize nuclear burning in different ways, which may explain the fact that no thermonuclear bursts have been observed to date from accreting NSs in high-mass X-ray binaries (HMXBs).

Although direct observational evidence of stable thermonuclear burning on accreting NSs has been elusive, as this is outshined by the much more efficient accretion-powered “persistent” emission, theoretical arguments and indirect observational evidence (Taam 1981; Fujimoto et al. 1981; van Paradijs et al. 1988; Lewin et al. 1993; Bildsten 1998) suggest that at very high \dot{m} , close to or above the Eddington mass accretion rate (Secs. 2 & 4), thermonuclear burning of the accreted H and He proceeds only stably. Near the transition between unstable and stable burning, an oscillatory burning regime was predicted by Paczynski (1983), known as marginally stable burning. Revnivtsev et al. (2001) discovered millihertz quasi-periodic oscillations (mHz QPOs) in the X-ray flux of three atoll sources (the sub-class of low luminosity NS-LMXBs; Hasinger & van der Klis 1989): 4U 1636–536, 4U 1608–52 and Aql X-1 (see also Strohmayer & Smith 2011). They attributed this new phenomenon to marginally stable burning on the NS surface. The mHz QPO frequency in one of these systems has been found to decrease with time until a bright type I X-ray burst occurs (Altamirano et al. 2008). The persistent luminos-

¹ Massachusetts Institute of Technology - Kavli Institute for Astrophysics and Space Research, Cambridge, MA 02139, USA

² Astronomical Institute “Anton Pannekoek”, University of Amsterdam and Center for High-Energy Astrophysics, PO BOX 94249, 1090 GE, Amsterdam, Netherlands

³ Department of Physics, McGill University, 3600 rue University, Montreal, QC H3A 2T8, Canada

⁴ School of Physics and Astronomy, University of Minnesota, 116 Church Street SE, Minneapolis, MN 55455, USA

⁵ Rubicon Fellow

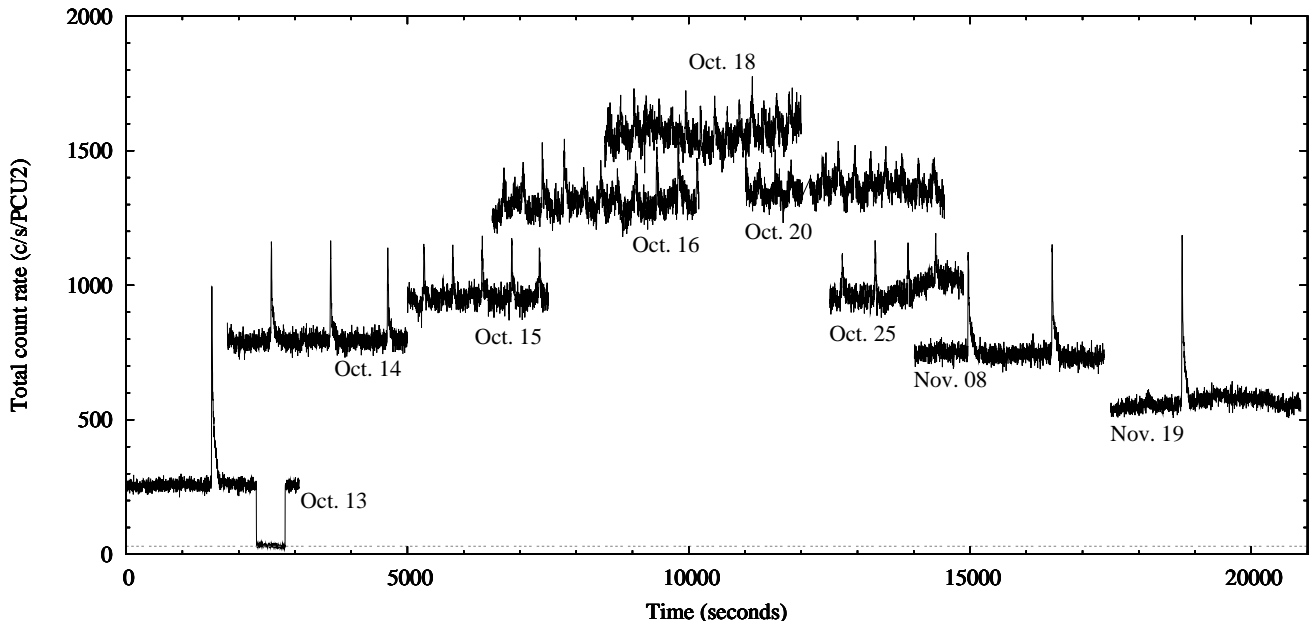


FIG. 1.— Overview of the burst and persistent emission evolution along the outburst of T5X2. Black lines show total 2 s time resolution light curves during one *RXTE* orbit for nine selected dates, as indicated (using PCU2 and the full $\sim 2\text{--}60$ keV band; gray dashed line shows the approximate, not subtracted, background rate). Times have been shifted arbitrarily for display purposes. The increase in burst rate and decrease in burst brightness as the persistent flux rises is evident. The step in October 13 was produced by a lunar eclipse (Strohmayer et al. 2010). The source became unobservable for *RXTE* after November 19 due to Solar constraints.

ity at which such mHz QPOs are observed has remained a puzzle, as it suggests a critical \dot{m} about an order of magnitude lower than the stability boundary predicted by theory (e.g., Heger et al. 2007b).

On 2010 October 10, an X-ray transient in the direction of the globular cluster Terzan 5 was discovered with the *International Gamma-ray Astrophysics Laboratory* (Bordas et al. 2010; Chenevez et al. 2010). During the following week, *Rossi X-ray Timing Explorer* (*RXTE*) observations revealed 11 Hz pulsations (Strohmayer & Markwardt 2010) and burst oscillations at the same frequency (Altamirano et al. 2010b; Cavecchi et al. 2011). The *Chandra* localization (Pooley et al. 2010) confirmed that this was a new NS transient, named IGR J17480–2446 (labeled CX25 or CXOGLb J174804.8–244648 by Heinke et al. 2006). We refer hereinafter to IGR J17480–2446 as T5X2, as this is the second bright X-ray source discovered in Terzan 5 (after EXO 1745–248). A 21.3 hr orbital period was measured from the Doppler shifts on the pulsar frequency (Strohmayer et al. 2010; Papitto et al. 2011), and the NS magnetic field was estimated to be between $10^8\text{--}10^{10}$ G based on the inferred magnetospheric radius (Papitto et al. 2011; Miller et al. 2011). This makes T5X2 the type I X-ray burst source (burster) with the slowest known NS spin and with the highest estimates of the NS magnetic field strength. Near the outburst peak T5X2 showed X-ray spectral and variability behavior typical of Z sources (the sub-class of high luminosity NS-LMXBs; Hasinger & van der Klis 1989), when it was accreting at about half of the Eddington rate (Altamirano et al. 2010c).

Linares et al. (2010a) argued that all the X-ray bursts from T5X2 had a thermonuclear origin, based on the evolution of the burst rate. Given the lack of spectral softening along the tail of many of the bursts

and their short recurrence times, Galloway & in’t Zand (2010) suggested that some of the T5X2 bursts were type II instead of type I (i.e., accretion- instead of nuclear-powered). However, the persistent-to-burst energy ratio throughout the October–November outburst of T5X2 was typical of type I X-ray bursts, i.e., fully consistent with the accretion-to-thermonuclear efficiency ratio (Linares et al. 2011; Chakraborty & Bhattacharyya 2011; Motta et al. 2011). Furthermore, Linares et al. (2011) measured a smooth evolution of the burst luminosity and spectral profiles and put forward a scenario to explain the lack of cooling in the faintest bursts, conclusively identifying all X-ray bursts detected from T5X2 as thermonuclear.

We present a thorough analysis of the mHz QPOs from T5X2, including but not limited to the ones originally reported by Linares et al. (2010a). We study the mHz QPO frequency evolution and energy-dependent amplitude, as well as all X-ray bursts from T5X2 detected with *RXTE* while the persistent (accretion) luminosity varied along the outburst. Unlike previous studies (Motta et al. 2011; Chakraborty & Bhattacharyya 2011), we analyze the complete sample of *RXTE* bursts and compare their properties to theoretical models of thermonuclear burning, along the full range in persistent luminosity ($\sim 10\text{--}50\%$ of the Eddington luminosity). Section 2 gives the details of the data analysis, and Section 3 presents the main observational results: a smooth evolution between bursts and mHz QPOs (Figure 1), the mHz QPO properties in detail and four different bursting regimes during the October–November 2010 outburst of T5X2. In Section 4 we place the unique mHz QPO and bursting behavior of T5X2 in the framework of thermonuclear burning theory and discuss the possible effects of composition, NS spin and magnetic field on the observed bursting properties. Section 5 gives our summary and conclusions.

2. DATA ANALYSIS

We analyzed all *RXTE* observations of T5X2 during its October–December 2010 outburst: a total of 46 observations taken between 2010 October 13 and 2010 November 19 (proposal-target number 95437-01). The source became Sun constrained after that date, and was not detected by the *Monitor of All-sky X-ray Image (MAXI)* on 2010 December 28, indicating that the outburst finished between 2010 November 19 and 2010 December 28. We visually searched for X-ray bursts in the full dataset, using 2 s time resolution 2–30 keV lightcurves. We performed time-resolved spectroscopy of all bursts using high time resolution data (E_125us_64M_0.1s, or GoodXenon when available). We extracted dead-time corrected spectra in 2 s time bins, using a ~ 100 s-long pre- or post-burst interval as background. We added a 1% systematic error to all channels, grouped them to a minimum of 15 counts per channel when necessary and fitted the resulting spectra within Xspec (v 12.6.0q), using a simple blackbody model with the absorbing column density fixed to $1.2 \times 10^{22} \text{ cm}^{-2}$ (Heinke et al. 2006). We used a distance to T5X2 of 6.3 kpc, the highest value reported from *HST* photometry of Terzan 5 (Ortolani et al. 2007), consistent with the distance measurement based on photospheric radius expansion bursts from another burster in the same globular cluster (Galloway et al. 2008). We note, however, that recent estimates of this distance range between 4.6 kpc and 8.7 kpc (Cohn et al. 2002; Ortolani et al. 2007; Lanzoni et al. 2010), and therefore any value of the luminosity, energy and mass accretion rate has a systematic uncertainty of a factor ~ 3.6 .

We measured the burst rise time (t_{rise} , as defined in Galloway et al. 2008, i.e., the time to go from 25% to 90% of the peak count rate), and the total radiated energy (E_b) by integrating the bolometric luminosity along each burst. We defined the wait time, t_{wait} , as the time elapsed between the peak of the previous burst and the peak of a given burst, available when no data gaps were present before the burst. We measured the daily-averaged burst recurrence time, t_{rec} , as the total exposure time during one day (excluding those orbits where no bursts are detected) divided by the number of bursts detected on that day. Therefore, the instantaneous and daily-averaged burst rate, ν_{burst} , are given by t_{wait}^{-1} and t_{rec}^{-1} , respectively. When only one burst was detected on a given day, we considered t_{rec} an approximate lower limit on the recurrence time. We also obtained daily averages of E_b , peak burst luminosity (L_{peak}), blackbody temperature (kT_{peak}) and radius (R_{peak}), following the same method described in Linares et al. (2011): peak burst values correspond to a 4 s long interval around the burst peak.

Due to the smooth evolution from a series of bursts into a mHz QPO and vice versa (see Fig. 1 and Sec. 3) the distinction between “frequent bursts” and mHz QPOs is, to some extent, arbitrary. We searched for mHz QPOs all observations taken when the daily-averaged burst recurrence time was shorter than 350 s, which corresponds to 10 observations between MJDs 55485–55490 (around the outburst peak). Given the typical duration of a continuous *RXTE* observation segment (an “orbit”), this threshold ensures that about 10 or more QPO cycles,

or bursts, are observed without interruption. To study the mHz QPOs in those *RXTE* orbits we used 2–60 keV 1 s-bin light curves from all active PCUs combined. We then calculated a Lomb-Scargle periodogram (LSP, oversampled by a factor of 3; Lomb 1976; Scargle 1982) for each light curve and measured the mHz QPO frequency, ν_{QPO} , as that frequency with the highest power in the periodogram. The corresponding period was then used to fold the background-corrected light curve (using background rates from *pcabackest* in 16-s steps) and produce a mHz QPO folded profile, from which we measured the fractional root-mean-squared (rms) amplitude. To investigate the energy dependence of the mHz QPO amplitude, we also produced light curves in five different energy bands (in keV: 2–3, 3–5.5, 5.5–9.5, 9.5–21 and 21–53), folded the light curve at the period found in the respective 2–60 keV range dataset and measured the “rms spectrum” of the mHz QPOs. We also performed 2048 s-long fast Fourier transforms (FFTs) using the 2–60 keV energy band and the same *RXTE* orbits, in order to constrain the mHz QPO coherence or “quality factor”.

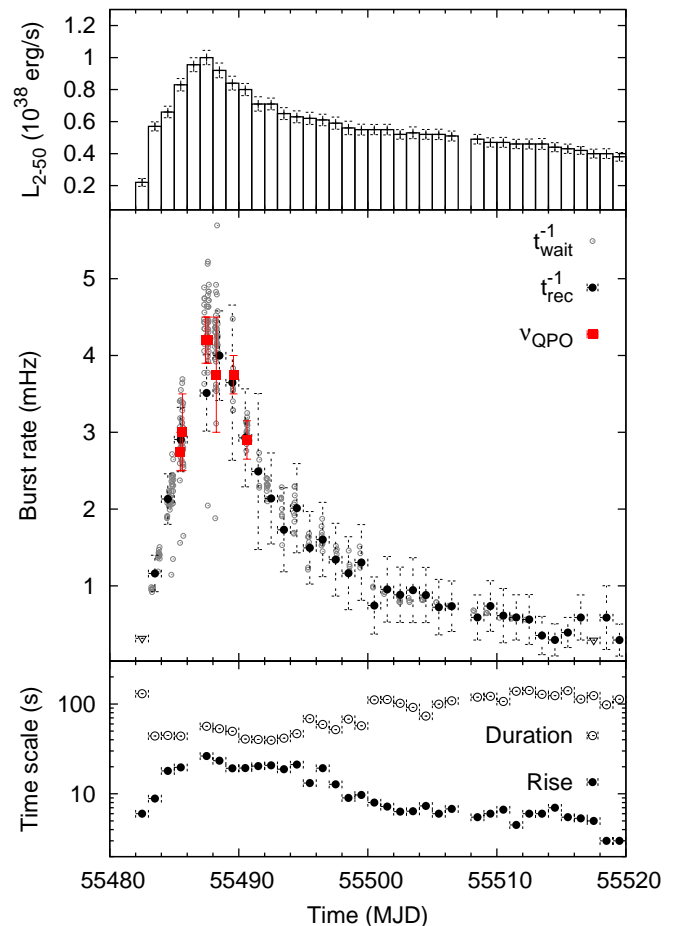


FIG. 2.— From top to bottom panels, evolution along the outburst of *i*) persistent 2–50 keV luminosity; *ii*) burst rate as measured from t_{wait} (open gray circles), t_{rec} (filled black circles) and mHz QPO frequency (red filled squares; see Sec. 2 for definitions) and *iii*) burst rise time and duration. Gray and black circles show individual burst measurements and daily averages, respectively. Open triangles show burst rate daily averages based on one single burst, which we consider as upper limits.

In order to measure the persistent (accretion) luminos-

TABLE 1
DAILY-AVERAGED BURST PROPERTIES AND PERSISTENT LUMINOSITY FROM T5X2.

Date ^a (MJD)	Exposure ^b (s)	Bursts ^c	t_{rec} ^d (s)	E_b ^e 10^{39} erg	L_{peak} ^e 10^{37} erg/s	kT_{peak} ^f (keV)	R_{peak} ^e (km)	L_{2-50} ^e 10^{37} erg/s
55482	3158	1	3158.0	1.60 ± 0.07	4.60 ± 0.57	2.27 ± 0.08	3.67 ± 0.23	2.20 ± 0.25
55483	20666	24	861.1	0.42 ± 0.01	2.00 ± 0.10	2.13 ± 0.03	2.70 ± 0.07	5.70 ± 0.28
55484	19709	42	469.3	0.28 ± 0.01	1.30 ± 0.07	2.01 ± 0.03	2.35 ± 0.07	6.60 ± 0.36
55485	16514	48	344.0	0.29 ± 0.01	1.30 ± 0.07	1.91 ± 0.02	2.69 ± 0.07	8.30 ± 0.39
55486	[17334]	[0]	-	-	-	-	-	9.55 ± 0.44
55487	14235 [6980]	50 [0]	284.7	0.36 ± 0.01	1.30 ± 0.08	1.72 ± 0.02	3.01 ± 0.10	10.00 ± 0.45
55488	11755 [3633]	47 [0]	250.1	0.37 ± 0.01	1.20 ± 0.07	1.69 ± 0.02	3.13 ± 0.09	9.20 ± 0.46
55489	3565 [3752]	13 [0]	274.2	0.31 ± 0.01	1.00 ± 0.11	1.77 ± 0.05	2.48 ± 0.14	8.40 ± 0.43
55490	7172	21	341.5	0.28 ± 0.01	1.10 ± 0.09	1.82 ± 0.03	2.65 ± 0.10	8.00 ± 0.38
55491	2410	6	401.7	0.23 ± 0.01	0.99 ± 0.16	1.60 ± 0.06	3.21 ± 0.26	7.10 ± 0.45
55492	6079	13	467.6	0.30 ± 0.01	1.30 ± 0.14	1.80 ± 0.05	2.75 ± 0.16	7.10 ± 0.37
55493	5780	10	578.0	0.24 ± 0.01	1.10 ± 0.13	1.59 ± 0.04	3.28 ± 0.20	6.50 ± 0.37
55494	5963	12	496.9	0.27 ± 0.01	1.20 ± 0.14	1.73 ± 0.05	2.95 ± 0.18	6.30 ± 0.37
55495	6685	10	668.5	0.51 ± 0.01	1.70 ± 0.11	1.90 ± 0.03	3.10 ± 0.11	6.20 ± 0.38
55496	6860	11	623.6	0.36 ± 0.01	1.30 ± 0.11	1.83 ± 0.04	2.79 ± 0.12	6.10 ± 0.36
55497	5964	8	745.5	0.37 ± 0.02	1.60 ± 0.15	1.97 ± 0.04	2.76 ± 0.13	5.90 ± 0.38
55498	5150	6	858.3	0.48 ± 0.02	1.60 ± 0.14	1.94 ± 0.04	2.95 ± 0.13	5.60 ± 0.42
55499	5364	7	766.3	0.35 ± 0.01	1.60 ± 0.13	1.96 ± 0.04	2.81 ± 0.11	5.50 ± 0.34
55500	5372	4	1343.0	0.74 ± 0.03	1.90 ± 0.17	1.98 ± 0.04	3.11 ± 0.14	5.50 ± 0.32
55501	5236	5	1047.2	0.79 ± 0.02	2.10 ± 0.16	2.02 ± 0.04	3.07 ± 0.11	5.50 ± 0.33
55502	6789	6	1131.5	0.87 ± 0.02	2.50 ± 0.15	2.06 ± 0.03	3.19 ± 0.10	5.20 ± 0.30
55503	5292	5	1058.4	0.74 ± 0.02	2.30 ± 0.16	2.11 ± 0.04	3.00 ± 0.10	5.30 ± 0.37
55504	6810	6	1135.0	0.57 ± 0.02	2.10 ± 0.14	2.15 ± 0.04	2.75 ± 0.09	5.20 ± 0.31
55505	5536	4	1384.0	0.74 ± 0.02	2.20 ± 0.18	2.12 ± 0.04	2.88 ± 0.12	5.20 ± 0.32
55506	6803	5	1360.6	0.93 ± 0.02	2.60 ± 0.17	2.14 ± 0.04	3.06 ± 0.10	5.10 ± 0.31
55508	6799	4	1699.8	1.00 ± 0.03	2.70 ± 0.19	2.18 ± 0.04	3.07 ± 0.10	4.90 ± 0.30
55509	6781	5	1356.2	1.06 ± 0.02	2.90 ± 0.16	2.21 ± 0.03	3.08 ± 0.08	4.70 ± 0.29
55510	4893	3	1631.0	1.02 ± 0.03	3.10 ± 0.23	2.08 ± 0.04	3.54 ± 0.13	4.70 ± 0.31
55511	6788	4	1697.0	1.26 ± 0.03	3.10 ± 0.20	2.07 ± 0.03	3.60 ± 0.11	4.60 ± 0.29
55512	5329	3	1776.3	1.28 ± 0.03	3.30 ± 0.21	2.17 ± 0.04	3.35 ± 0.11	4.60 ± 0.31
55513	5661	2	2830.5	1.37 ± 0.05	3.30 ± 0.37	2.30 ± 0.07	3.01 ± 0.17	4.60 ± 0.34
55514	6737	2	3368.5	1.46 ± 0.03	3.70 ± 0.26	2.25 ± 0.04	3.32 ± 0.12	4.40 ± 0.28
55515	10197	4	2549.2	1.33 ± 0.02	3.70 ± 0.18	2.23 ± 0.03	3.40 ± 0.08	4.30 ± 0.29
55516	6803	4	1700.8	1.37 ± 0.03	3.70 ± 0.25	2.16 ± 0.04	3.61 ± 0.12	4.20 ± 0.24
55517	3410	1	3410.0	1.42 ± 0.04	3.70 ± 0.29	2.21 ± 0.04	3.47 ± 0.13	4.00 ± 0.28
55518	3407	2	1703.5	1.22 ± 0.03	3.80 ± 0.26	2.31 ± 0.04	3.24 ± 0.11	4.00 ± 0.30
55519	6788	2	3394.0	1.45 ± 0.04	3.90 ± 0.34	2.19 ± 0.05	3.61 ± 0.16	3.80 ± 0.27

^aMJD 55482 is 2010 October 13, and MJD 55519 is 2010 November 19.

^bTotal daily exposure time in data segments (orbits) where bursts are detected. The total daily exposure time for segments without detected bursts is indicated between square brackets (whenever this time is larger than the burst recurrence time). Thus square brackets indicate periods of intrinsic burst cessation.

^cTotal number of bursts detected per day. Square brackets indicate periods of intrinsic burst cessation, when no bursts were detected despite long enough exposure time.

^dDaily-averaged burst recurrence time.

^eBolometric integrated burst energy (E_b) and peak burst luminosity (L_{peak}). Persistent luminosity (L_{2-50}) in the 2–50 keV energy band (see Sec. 2 for bolometric correction). Peak burst blackbody radius (R_{peak}) not color- or redshift-corrected. All use a distance of 6.3 kpc.

^fPeak burst blackbody temperature.

ity, we extracted one dead-time-corrected spectrum per observation from Standard 2 data, excluding all bursts and subtracting the background spectrum estimated with the bright source background model and *pcabackest* (v. 3.8). We then fitted each persistent spectrum with a model consisting of a disk blackbody, a power law and a Gaussian line with energy fixed at 6.5 keV, correcting for absorption as above. We calculated the 2–50 keV persistent luminosity (L_{2-50}) from the best fit model. Furthermore, we measured the 0.01–2 keV unabsorbed flux from a simultaneous fit to the T5X2 spectrum measured by *Swift*-XRT (0.5–10 keV) and *RXTE*-PCA (2.5–25 keV) on MJD 55501 (2010 November 01), extrapolating the *phabs*simpl(bbody + diskbb)* best fit model down to 0.01 keV, and found a bolometric correction factor

of 1.13. This bolometric correction factor converts 2–50 keV into 0.01–50 keV flux, which we take as bolometric flux given that the persistent spectrum remains soft (photon index 2.4–3.3) throughout the outburst and we therefore do not expect sizeable emission above 50 keV (with the only exception of the first observation, when T5X2 was in the hard state and the photon index was ~ 1.7). Using the same procedure, we found a bolometric correction factor of 1.02 for the 0.5–50 keV luminosity from Cir X-1 reported by Linares et al. (2010b, used in Sec. 4). We applied these bolometric correction factors in order to estimate the bolometric persistent luminosity: L_{pers} . We use throughout this work an Eddington luminosity of $L_{\text{Edd}} = 2.5 \times 10^{38} \text{ erg s}^{-1}$ to calculate Eddington-normalized L_{pers} . To convert from L_{pers} to \dot{m} , we as-

sume homogeneous accretion onto the NS and that the (general-relativistic) gravitational energy of the in-falling matter is fully converted into radiation at the surface of a $1.4 M_{\odot}$ mass, 10 km radius NS. We define the Eddington mass accretion rate per unit area, \dot{m}_{Edd} , as the mass accretion rate needed to sustain a luminosity equal to L_{Edd} . With this definition $\dot{m}_{\text{Edd}} = 1.2 \times 10^5 \text{ g cm}^{-2} \text{ s}^{-1}$.

3. RESULTS

We found and analyzed a total of 398 X-ray bursts occurring between 2010 October 13 and 2010 November 19, including the faint and frequent bursts near the peak of the outburst that form the mHz QPOs (see below). We show in Figure 1 an overview of the joint evolution of persistent emission and burst properties along the T5X2 outburst. Bursts become more frequent and fainter when the persistent luminosity, L_{pers} , increases, and they turn into brighter and more frequent bursts during the outburst decay. Most interestingly, the X-ray bursts gradually develop into the observed mHz QPO during the outburst rise, and the mHz QPO mutates into a series of bursts along the outburst decay (Figure 1), an unprecedented phenomenon among thermonuclear bursters. This also makes T5X2 the most prolific source of thermonuclear bursts known to date (an average burst rate over more than a month of 4.9 hr^{-1} ; 5.5 hr^{-1} excluding orbits where no bursts were detected), with the shortest recurrence times between thermonuclear bursts observed to date (as short as $\sim 200 \text{ s}$; c.f. Linares et al. 2009; Keek et al. 2010).

The *smooth metamorphosis* between bursts and mHz QPOs can be seen qualitatively in Figure 1, and quantitatively by studying the evolution of several burst properties (Figure 2 & Table 1). Burst rate, rise time and duration as well as peak burst luminosity, L_{peak} , and total radiated energy E_b ; (see also Linares et al. 2011), all evolve gradually while L_{pers} changes by a factor of ~ 5 along the outburst. Figure 2 (middle panel) also shows that the burst rate equals the mHz QPO frequency during the outburst peak, $\nu_{\text{burst}} = \nu_{\text{QPO}}$, as expected given that the mHz QPOs are simply formed by a series of faint and frequent bursts. This unique behavior makes the distinction between bursts and mHz QPOs somewhat arbitrary. As explained in Section 2, our practical definition of mHz QPO requires burst recurrence times shorter than 350 s, so that typically 10 or more QPO cycles are observed without interruption. In a few occasions we find

that one burst is missing from the series of regular bursts, and the corresponding values of $\nu_{\text{burst}} = t_{\text{wait}}^{-1}$ for individual bursts are a factor ~ 2 lower than the general trend, as can be seen in Figure 2 (middle panel). Interestingly, a similar behavior with sporadic “missing bursts” is seen in the mHz QPO simulations presented in Heger et al. (2007b).

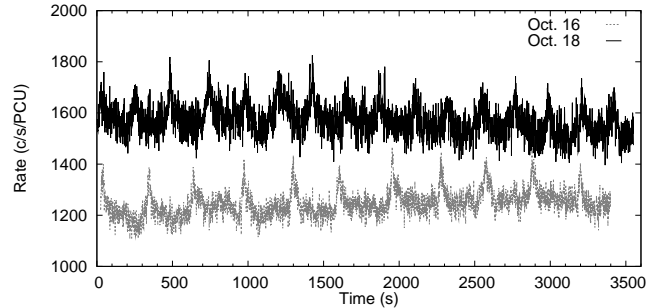


FIG. 3.— Light curves of the mHz QPOs on October 16 (gray) and 18 (black), in the 2–60 keV energy band, using 1-s time bins and no background subtraction. One *RXTE* orbit is shown in each case, and time is relative to the start of that orbit (2010-10-16 14:33:27 UTC and 2010-10-18 15:09:55 UTC). The persistent luminosity was higher on October 18 ($L_{\text{pers}} \simeq 0.45 L_{\text{Edd}}$) than October 16 ($L_{\text{pers}} \simeq 0.38 L_{\text{Edd}}$). To illustrate this, count rate is normalized to the number of active PCUs.

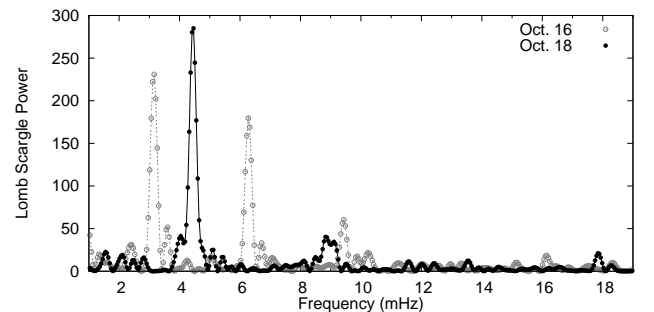


FIG. 4.— Lomb-Scargle periodograms of the mHz QPOs on October 16 (gray) and 18 (black), showing the QPO harmonic structure and the change in ν_{QPO} .

3.1. mHz QPOs

We report the discovery of several instances of mHz QPOs during the peak of the T5X2 outburst, on 2010 October 16, 18, 19, 20 and 21 (MJDs 55485–55490; Linares et al. 2010a, for the initial report of mHz QPOs on 2010 October 18 and 19). Two examples of mHz QPO light curves are shown in Figure 3, each spanning one *RXTE* orbit. Table 2 shows the main QPO properties: fractional rms amplitudes between 1.3% and 2.2% (in the 2–60 keV band) and ν_{QPO} in the range 2.8–4.2 mHz (note that the lower end of this frequency range corresponds to our mHz QPO definition, Secs. 2 & 3). Figure 4 presents LSPs of two cases, on October 16 and 18, clearly showing the change in ν_{QPO} as well as the harmonic structure (up to 4 overtones are visible in the LSPs). By inspecting the power spectra obtained from 2048-s-long FFTs, we find that the mHz QPO power is in all cases spread over one

TABLE 2
PROPERTIES OF THE mHz QPOs FROM T5X2.

Date (MJD)	OBSID ^a	ν_{QPO} (mHz)	rms _{QPO} (%)	$L_{\text{pers}}/10^{37}$ (erg/s)	$\dot{m}/10^4$ ($\text{g cm}^{-2} \text{ s}^{-1}$)
55485.46	04-00 [1]	2.75 ± 0.2	1.9 ± 0.1	9.1 ± 0.4	4.5 ± 0.2
55485.63	04-01 [1,2,3]	3 ± 0.5	2.2 ± 0.1	9.9 ± 0.4	4.9 ± 0.2
55487.43	06-000 [1,4]	4.2 ± 0.2	1.3 ± 0.1	11.4 ± 0.4	5.6 ± 0.2
55487.62	06-00 [1,2]	4.2 ± 0.2	1.7 ± 0.2	12.1 ± 0.5	6.0 ± 0.2
55488.26	07-00 [1]	4.0 ± 0.5	1.4 ± 0.1	12.0 ± 0.5	5.9 ± 0.2
55489.59	08-00 [1]	3.75 ± 0.2	2.1 ± 0.1	9.6 ± 0.5	4.8 ± 0.2
55490.63	09-00 [1,2]	2.9 ± 0.2	2.2 ± 0.1	9.1 ± 0.4	4.5 ± 0.2

^aFor comparison, the reported values for the “low- L_{pers} mHz QPOs” are in the following ranges: $\nu_{\text{QPO}} = [7\text{--}14.3] \text{ mHz}$; rms_{QPO} = [0.7–1.9]% (2–5 keV); $L_{\text{pers}} = [0.6\text{--}3.5] \times 10^{37} \text{ erg/s}$ (Sec. 4.2; Revnivtsev et al. 2001; Altamirano et al. 2008).

^bcObservation (from proposal-target 95437-01) where the mHz QPOs are detected, orbit numbers used indicated between square brackets.

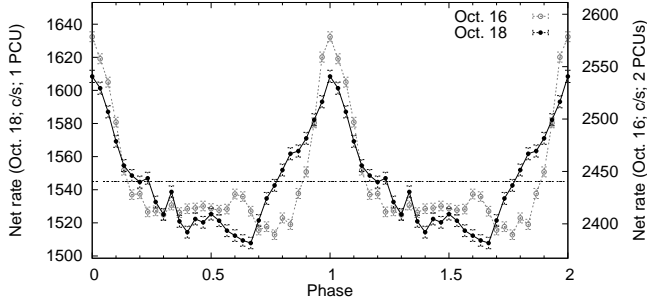


FIG. 5.— Folded background-subtracted 2–60 keV light curves of the mHz QPOs on October 16 (gray) and 18 (black). Peaks are at phase 0 by definition. Two QPO cycles are shown for clarity. Two PCUs were active on October 16, yielding a higher collected rate. The dashed horizontal line shows the average count rate, and the vertical range corresponds to 10% of that value in each case, showing that the fractional amplitude was higher on October 16 (Table 2). The net peak burst luminosity was in both cases $\simeq 1.3 \times 10^{37}$ erg s $^{-1}$ (Table 1).

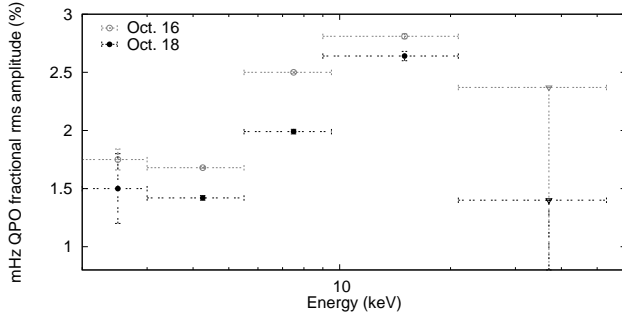


FIG. 6.— “RMS spectrum” of the mHz QPOs on October 16 (gray) and 18 (black). Their fractional rms amplitude increases with energy up to ~ 20 keV. No mHz QPOs are detected above that energy, empty triangles show upper limits on their fractional rms amplitude.

or two frequency bins, from which we derive a limit on the full-width-at-half-maximum, $\text{FWHM} \lesssim 1$ mHz. For the 2.8–4.2 mHz QPO frequencies this corresponds to a lower limit on the quality factor ($Q \equiv \nu_{\text{QPO}}/\text{FWHM}$) of $Q \gtrsim 3$, which reveals a fairly coherent QPO (a fairly constant t_{wait}).

We present in Figure 5 light curves folded at the mHz QPO period, showing folded burst/QPO profiles for the same two dates, October 16 and 18. In both cases the burst/QPO profile is peaked and highly non-sinusoidal (as seen also in the raw, unfolded light curves; Fig. 3), which explains the harmonic content. On October 18, when ν_{QPO} was highest (Table 2), we find a nearly symmetric burst/QPO profile. On October 16 the burst/QPO profile is slightly asymmetric, with the rise faster than the decay. We measure a mHz QPO fractional rms amplitude in the range 1.3–2.2 %, in the total (~ 2 –60 keV) PCA band. Furthermore, from our measurements of the mHz QPO amplitude at different energies (Sec. 2; Fig. 6) we find that its fractional rms amplitude increases between ~ 2 and ~ 20 keV, from $\sim 1.4\%$ to $\sim 2.8\%$ in the two cases presented in Figure 6. At energies higher than 20 keV the mHz QPO is not visible by naked eye in the light curves, nor it is conclusively detected using LSPs, FFTs or folded light curves. The

presence of red noise with variable strength gives rise to different upper limits on the fractional rms amplitude of the mHz QPO above 20 keV (between 1.4% and 3%; Fig. 6). As discussed in Section 4.2, such increase in QPO amplitude up to 20 keV is in contrast with mHz QPOs from other bursting NSs, which showed a fractional amplitude decreasing with increasing energy between 2 and 5 keV (Revnivtsev et al. 2001).

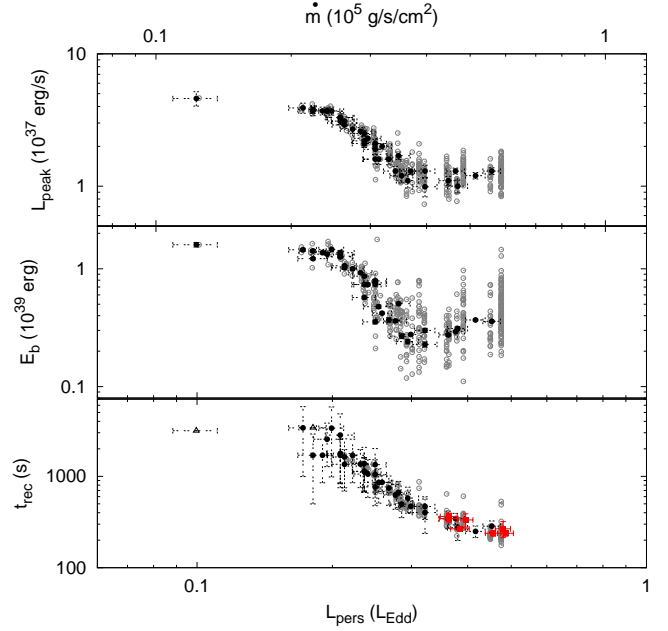


FIG. 7.— Burst peak luminosity (*top*), integrated burst energy (*middle*) and burst recurrence time, t_{rec} (*bottom*) vs. bolometric persistent luminosity (L_{pers}). Gray and black circles show individual burst measurements and daily averages, respectively. Red filled squares show recurrence times measured from the inverse of the mHz QPO frequency. The top axis shows the inferred \dot{m} assuming homogeneous accretion onto a $1.4 M_{\odot}$, 10 km radius NS (Sec. 2).

TABLE 3
BROKEN POWER LAW FITS TO THE BURST PROPERTIES VS. PERSISTENT LUMINOSITY RELATIONS.

Relation ^a	$L_{\text{peak}}-L_{\text{pers}}$	$E_{\text{b}}-L_{\text{pers}}$	$t_{\text{rec}}-L_{\text{pers}}$
[range]	[0.1–0.3]	[0.1–0.3]	[0.17–0.45]
K^{b}	2.2 ± 0.7	0.9 ± 0.1	10 ± 7
i_1	-0.3 ± 0.2	-0.2 ± 0.1	-3.2 ± 0.5
$L_{\text{break}}(L_{\text{Edd}})$	0.20 ± 0.01	0.20 ± 0.01	0.33 ± 0.04
i_2	-2.7 ± 0.1	-4.4 ± 0.1	-1.0 ± 0.9
χ^2 / dof	$38.5 / 25$	$930 / 25$	$6.1 / 30$

^aPairs of variables fitted with a broken power law: L_{peak} , E_{b} and t_{rec} vs. L_{pers} (see Figures 7 & 8). The L_{pers} range used in each fit is quoted between brackets, in units of L_{Edd} . i_1 and i_2 represent, respectively, the power law indices before and after the break (at L_{break}).

^bPower law normalization before the break, same units as L_{peak} (10^{37} erg s $^{-1}$), E_{b} (10^{39} erg) and t_{rec} (s).

3.2. Burst properties vs. accretion rate

We present in this Section the relation between burst properties and \dot{m} , as inferred from L_{pers} , including the

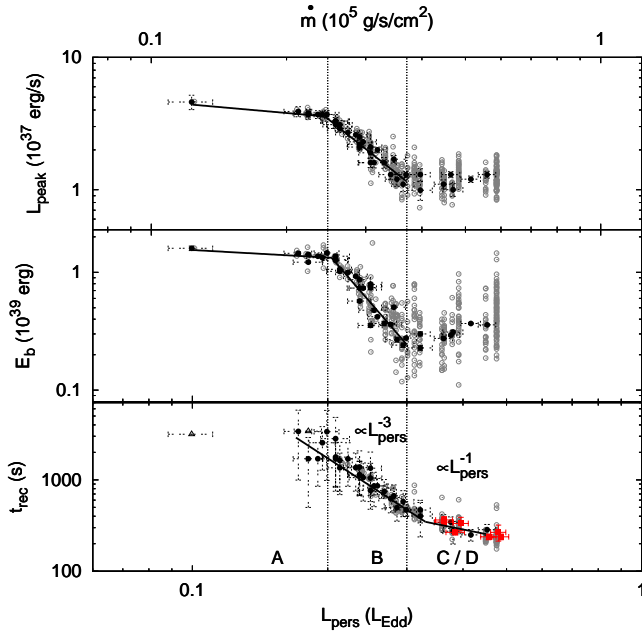


FIG. 8.— Same as Figure 7, showing also the broken power law fits to the L_{peak} , E_b , t_{rec} vs. L_{pers} relations (Table 3). Three regimes are apparent and labeled along the bottom axis: slow decrease (at $L_{\text{pers}}/L_{\text{Edd}} < 0.2$; regime A), fast drop (at $0.2 < L_{\text{pers}}/L_{\text{Edd}} < 0.3$; regime B) and saturation ($L_{\text{pers}}/L_{\text{Edd}} > 0.3$; regime C) of the L_{peak} , E_b vs. L_{pers} relations. The t_{rec} values follow approximate $t_{\text{rec}} \propto L_{\text{pers}}^{-3}$ and $t_{\text{rec}} \propto L_{\text{pers}}^{-1}$ relations in regimes B and C, as indicated (see Figure 11, Table 4 and Secs. 3.2 & 4).

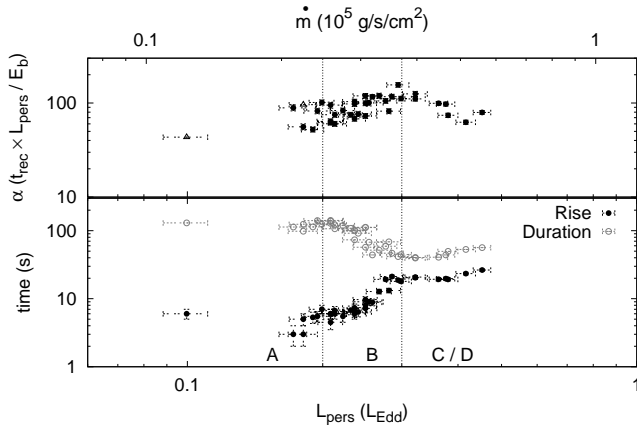


FIG. 9.— Daily-averaged accretion-to-burst energy ratio (α , top panel) and burst time scales (rise time and duration, bottom panel) vs. persistent luminosity (L_{pers}) during the T5X2 outburst. Open triangles represent lower limits (one single burst detected during that day). The corresponding bursting regimes are indicated with dotted lines and labels along the bottom axis (Table 4).

faintest and most frequent bursts which form the mHz QPOs (see above). Figure 2 shows L_{peak} , E_b and t_{rec} as a function of the Eddington-normalized L_{pers} and \dot{m} (Sec. 2). The overall trend is that of an anti-correlation between L_{peak} , E_b and t_{rec} on the one hand and L_{pers} on the other (see also Fig. 1 in Linares et al. 2011; Motta et al. 2011). Closer inspection of the burst properties over the full L_{pers} range (0.1 – $0.5 L_{\text{Edd}}$; see Figure 7) reveals a more complex and interesting behavior, namely,

four different bursting regimes.

- At the lowest persistent luminosities, $0.1 < L_{\text{pers}}/L_{\text{Edd}} < 0.2$, when L_{pers} increases both L_{peak} and E_b (and possibly t_{rec}) decrease moderately, from $L_{\text{peak}} \simeq 4.6 \times 10^{37} \text{ erg/s}$, $E_b \simeq 1.6 \times 10^{39} \text{ erg}$ to $L_{\text{peak}} \simeq 3.7 \times 10^{37} \text{ erg/s}$, $E_b \simeq 1.3 \times 10^{39} \text{ erg}$. We refer to this 0.1 – $0.2 L_{\text{Edd}}$ regime as *slow decrease*, or *regime A* (see Fig. 7).
- At higher persistent luminosities, $0.2 < L_{\text{pers}}/L_{\text{Edd}} < 0.3$, we find L_{peak} and E_b to be steeply anticorrelated with L_{pers} , while t_{rec} also decreases from 200 s to 400 s with increasing L_{pers} . We refer to this 0.2 – $0.3 L_{\text{Edd}}$ regime as *fast drop*, or *regime B* (see Fig. 7).
- At the highest persistent luminosities ($L_{\text{pers}} > 0.3 L_{\text{Edd}}$), when mHz QPOs are detected, burst peak luminosity and energy reach approximately constant values (*saturation*, or *regime C*): $L_{\text{peak}} \simeq 1.2 \times 10^{37} \text{ erg/s}$ and $E_b \simeq 0.3 \times 10^{39} \text{ erg}$. The burst recurrence time, however, keeps decreasing with increasing L_{pers} from $t_{\text{rec}} \simeq 400$ s down to ~ 240 s on 2010 October 18 (Fig. 7; Table 2).
- Finally, during incursions into the flaring/normal branches near the outburst peak, when T5X2 showed Z source behavior (Altamirano et al. 2010c), neither bursts nor mHz QPOs were detected. These few episodes without bursting activity, which we refer to as *regime D*, were associated with moderate ($\sim 30\%$) short (hour-long) drops in L_{pers} and occurred between MJDs 55486 and 55496 (while $L_{\text{pers}} \gtrsim 0.3 L_{\text{Edd}}$). They are noted with square brackets in Table 1.

Interestingly, regimes C and D show similar L_{pers} (0.3 – $0.5 L_{\text{Edd}}$), but their variability and spectral properties differ (i.e., they constitute different “accretion states”; see Altamirano et al. 2012, in prep.). We summarize the main bursting properties of all four regimes in Table 4.

In order to quantify the anticorrelations explained above and to characterize the bursting regimes present in T5X2, we fit the L_{peak} , E_b , t_{rec} vs. L_{pers} relations with broken power law functions. The results are shown in Figure 8 and Table 3, and confirm that the two “breaks” or transitions occur at $L_{\text{pers}} \simeq 0.2 L_{\text{Edd}}$ and $L_{\text{pers}} \simeq 0.3 L_{\text{Edd}}$. Due to the large scatter some of the fits are statistically poor, yet they allow us to constrain the slope and transition luminosity of the three bursting regimes (Fig. 8). Remarkably, the t_{rec} – L_{pers} relation that we find in regime B ($L_{\text{pers}} \sim 0.2$ – $0.3 L_{\text{Edd}}$) is far from linear, as would be expected from a $t_{\text{rec}} \propto \dot{m}^{-1}$ relation if $\dot{m} \propto L_{\text{pers}}$ (See Sec. 4.1 for further discussion). Instead, it is close to $t_{\text{rec}} \propto L_{\text{pers}}^{-3}$: we measure a t_{rec} – L_{pers} power law index in regime B of -3.2 ± 0.5 (see further discussion in Sec. 4). We also calculate the mean alpha parameter ($\alpha \equiv L_{\text{pers}} \times t_{\text{rec}} / E_b$) from the daily-averaged values reported by Linares et al. (2011) and, after applying the bolometric correction we obtained from broadband X-ray spectral fits (Sec. 2), we find a mean α of 102, with a standard deviation of 27. Figure 9 shows that α increases from ~ 60 to ~ 120 with increasing L_{pers} until

TABLE 4
SUMMARY OF BURSTING REGIMES IN T5X2. SEE SECTION 3.2 FOR DETAILS.

Regime	L_{pers} (L_{Edd})	t_{rec} (s)	E_{b} (10^{39} erg)	L_{peak} (10^{37} erg s $^{-1}$)	Description
A	0.1–0.2	>2000	1.6–1.3	4.6–3.7	Slow decrease of E_{b} & L_{peak} (and $t_{\text{rec}}?$) with increasing L_{pers} .
B	0.2–0.3	2000–400	1.3–0.3	3.7–1.2	Fast drop of t_{rec} , E_{b} & L_{peak} with increasing L_{pers} . $t_{\text{rec}} \propto L_{\text{pers}}^{-3}$.
C	0.3–0.5	400–200	~ 0.3	~ 1.2	Bursts evolve into mHz QPOs with increasing frequency ($t_{\text{rec}} \propto L_{\text{pers}}^{-1}$). E_{b} & L_{peak} “saturate”.
D	0.3–0.5	-	-	-	No bursts/mHz QPOs detected on normal & flaring branch in Z source phase.

$L_{\text{pers}} \simeq 0.3 L_{\text{Edd}}$ (regimes A & B), and decreases at higher luminosities (regime C) to reach again values close to 60. Figure 9 also shows the burst duration and rise time as a function of L_{pers} : the general trend is for bursts to become shorter and have slower rise when L_{pers} increases.

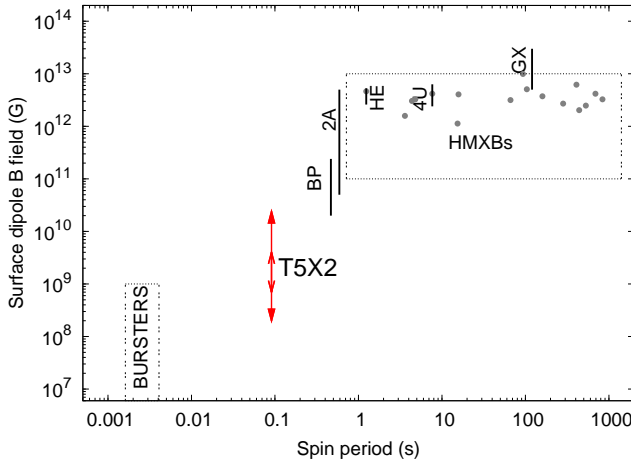


FIG. 10.— Magnetic field strength vs. spin period in accreting NSs. The dotted rectangle in the lower left corner (labeled ‘bursters’) shows the location of all previously known thermonuclear burst sources with measured spin (Psaltis & Chakrabarty 1999; Chakrabarty et al. 2003; Patruno 2010, and references therein). The dotted rectangle in the upper right corner (labeled ‘HMXBs’) shows the location of X-ray pulsars in high-mass X-ray binaries (Bildsten et al. 1997; filled gray circles show X-ray pulsars with B measured from cyclotron lines, Caballero & Wilms 2011). Red double-head arrows show the location of T5X2 (using the two magnetic field estimates from Papitto et al. 2011; Miller et al. 2011). Vertical black lines mark the location of other slow pulsars in LMXBs ($P_s > 0.01$ s), none of which has shown thermonuclear bursts to date. These are labeled with the first two characters of the source names, which follow: 2A 1822–371 (Jonker & van der Klis 2001), 4U 1626–67 (Rappaport et al. 1977; Orlandini et al. 1998), GRO 1744–28 (the “bursting pulsar”, BP; Kouveliotou et al. 1996; Finger et al. 1996; Cui 1997; Sturmer & Dermer 1996), Her X-1 (Truemper et al. 1978; Bildsten et al. 1997; Mihara et al. 1990; dal Fiume et al. 1998) and GX 1+4 (Chakrabarty & Roche 1997; Hinkle et al. 2006; Cui 1997).

4. DISCUSSION

The bursting behavior of T5X2 strikes as surprising for several reasons. During the last three decades

bursts at persistent luminosities $L_{\text{pers}} \gtrsim 0.2 L_{\text{Edd}}$ had proven exceptional and extremely difficult to detect, even when studying a large sample of bursters (e.g. Cornelisse et al. 2003; Galloway et al. 2008, and references therein). This decrease of burst rate at high L_{pers} , opposite to what standard burst theory predicts (Fujimoto et al. 1981; Bildsten 1998), has been attributed in the literature to several effects, including: i) stable thermonuclear burning becoming more important at high \dot{m} and consuming an increasing fraction of the accreted fuel (van Paradijs et al. 1988); ii) deflagration fronts or “flames” propagating on the NS surface and consuming part of the fuel (Bildsten 1995) and iii) non-spherical accretion confined to a fraction of the NS surface that would increase with L_{pers} (Bildsten 2000). The large number of bursts observed from T5X2 in October–November 2010 (at an average burst rate over more than a month of 4.9 hr^{-1} ; Sec. 3) make T5X2 the most prolific source of thermonuclear bursts known to date. Notably, such copious burst activity was observed when L_{pers} was in the range $0.1\text{--}0.5 L_{\text{Edd}}$, a regime where burst rate is found to decrease drastically in all other bursters. The only source that has shown (albeit sporadically) such high burst rates at similar L_{pers} is Cir X-1: on May 2010 it featured burst recurrence times as short as 1000–2000 s, when L_{pers} was $\sim 0.2 L_{\text{Edd}}$ (Linares et al. 2010b). Two other well known sources of “high- \dot{m} ” bursts, GX 17+2 and Cyg X-2, have shown bursts much less frequently (mean burst rate over more than 10 yr was 0.05 and 0.1 hr^{-1} , respectively; Galloway et al. 2008) and when L_{pers} was close to L_{Edd} . Other systems have shown thermonuclear bursts at intermediate accretion rates ($L_{\text{pers}} \simeq 0.1\text{--}0.5 L_{\text{Edd}}$; including GX 3+1, GX 13+1, Ser X-1, 4U 1636–53, 4U 1735–44, 4U 1746–37), but only sporadically (t_{wait} of at least one hour and typically much longer; Galloway et al. 2008, and references therein). T5X2 is therefore exceptional in that it follows the expected burst rate at high \dot{m} (Fujimoto et al. 1981; Bildsten 1998) much more closely than any other known burster (Cornelisse et al. 2003; Galloway et al. 2008). We extend on this comparison between thermonuclear burning theory and T5X2 in Section 4.1.

Moreover, T5X2 is the first slow X-ray pulsar (spin period $P_s > 10$ ms) to show thermonuclear bursts. None of the slower ($P_s \gtrsim 1$ s) “classical” X-ray pulsars in HMXBs have shown thermonuclear bursts to date, even if their persistent luminosity varies over the same range as in

bursters. This is usually attributed to the stronger dipolar NS magnetic field (B) in HMXBs channeling the accretion flow into a much smaller area than LMXBs, leading to stable burning of all the accreted fuel due to a very high local \dot{m} (Joss & Li 1980; see also Sec. 4.3). On the other hand, only 7 out of the more than 90 bursters known have shown X-ray pulsations in the persistent emission (i.e., 7 out of the 14 accreting millisecond pulsars have shown bursts to date). Before the discovery of T5X2 the slowest spinning burster had a spin frequency more than 20 times higher than T5X2 (IGR J17511–3057, with a spin frequency $\nu_s=245$ Hz; Markwardt et al. 2009; Altamirano et al. 2010a). T5X2 therefore bridges the gap between “pulsars that don’t burst and bursters that don’t (typically) pulse” (Bildsten 1998, and references therein). We show this in Figure 10 by comparing both the B and P_s values of T5X2 to those of LMXBs (including a few peculiar LMXBs) and HMXBs. Figure 10 clearly shows that T5X2 features values of B and P_s intermediate between bursters and HMXBs. We discuss the consequences of such a high B and long P_s for thermonuclear burst regimes in Sections 4.3 and 4.4, respectively.

The shortest burst wait times known to date (Linares et al. 2009; Keek et al. 2010, 5.4 and 3.8 min, respectively) were based on sets of typically two or three consecutive bursts followed by much longer periods without bursts. The bursts from T5X2 presented herein are remarkably quasi-periodic, not only in the mHz QPO phase, as witnessed by the well defined and smoothly evolving wait time in individual bursts (t_{wait} ; see Figs. 1 & 2). This behavior is analogous to the “clocked burster” (GS 1826–24; Tanaka 1989; Ubertini et al. 1999; Galloway et al. 2004; Heger et al. 2007a) and IGR J17511–3057 (Falanga et al. 2011), which have shown bursts at regular intervals with an approximate $t_{\text{rec}} \propto L_{\text{pers}}^{-1}$ relation, although at lower accretion rates than T5X2. For this reason, we compare in Figure 11 the burst energies and recurrence times of T5X2 to those of these two sources, as well as Cir X-1. The bursts from T5X2 (at $\dot{m} \sim 0.1\text{--}0.5 \dot{m}_{\text{Edd}}$) are more frequent and less energetic than those from GS 1826–24 and IGR J17511–3057 (at $\dot{m} \sim 0.02\text{--}0.06 \dot{m}_{\text{Edd}}$). Figure 11 also shows that the $t_{\text{rec}} \propto L_{\text{pers}}^{-3}$ relation that we find in regime B is unique to T5X2. The bursts from Cir X-1, however, have again a strong resemblance to those of T5X2, with energies in the same range ($\lesssim 10^{39}$ erg) and a similar $E_b\text{--}L_{\text{pers}}$ relation (a break or transition is also suggested by the Cir X-1 data; Figure 11).

4.1. Bursting regimes vs. burning regimes: the need for heat

In the present Section we compare in detail the T5X2 burst properties with theoretical predictions. Models of nuclear burning in the envelope of (non-magnetic, non-rotating) accreting NSs predict four different burning regimes on a NS accreting a mixture of hydrogen (H; mass fraction X_0), helium (He; mass fraction Y_0) and heavy elements (mainly CNO, mass fraction Z ; see Woosley & Taam 1976; Fujimoto et al. 1981; Taam 1981; Bildsten 1998; Cumming & Bildsten 2000, and references therein). At the highest accretion rates, close to or higher

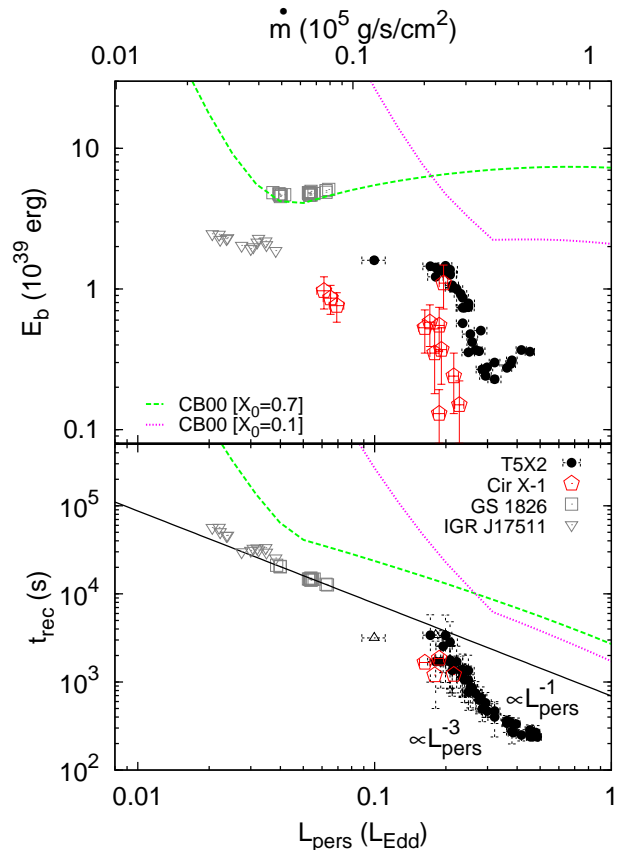


FIG. 11.— Burst energy (*top panel*) and recurrence time (*bottom panel*) vs. persistent luminosity (*bottom axis*) and inferred mass accretion rate per unit surface (*top axis*) for four bursters, as indicated on the bottom panel: T5X2 (filled black circles; this work), GS 1826–24 (“the clocked burster”, open gray squares; from Galloway et al. 2004), Cir X-1 (open red pentagons; from Linares et al. 2010b) and IGR J17511–3057 (open gray triangles; from Falanga et al. 2011). The solid line shows the empiric $t_{\text{rec}} \propto L_{\text{pers}}^{-1.05}$ relation found for GS 1826–24 by Galloway et al. (2004), similar to the $t_{\text{rec}} \propto L_{\text{pers}}^{-1.1}$ relation found in IGR J17511–3057 (Falanga et al. 2011). We also show the $E_b\text{--}\dot{m}$ and $t_{\text{rec}}\text{--}\dot{m}$ relations predicted by two ignition models from Cumming & Bildsten (2000, labeled CB00) with different accreted hydrogen fractions: $X_0=0.7$ (green dashed line) and $X_0=0.1$ (magenta dotted line). In both models the metallicity was assumed to be $Z=0.02$ and the heat flux from the crust was fixed at $Q_b=0.1$ MeV nucleon $^{-1}$.

than \dot{m}_{Edd} , both H and He burn stably and no bursts are expected (Sec. 4.2). For accretion rates

$$\dot{m} > \dot{m}_{\text{sHb}} \simeq 0.008 \dot{m}_{\text{Edd}} \left(\frac{0.7}{X_0} \right) \left(\frac{Z}{0.01} \right)^{1/2}, \quad (1)$$

(Bildsten 1998, where we assumed an opacity of $0.04 \text{ cm}^2 \text{ g}^{-1}$ and the value of \dot{m}_{Edd} given in Sec. 2), H burns stably between bursts at a constant rate, via the so-called (β -limited) “hot-CNO” cycle (Bildsten 1998; Cumming & Bildsten 2000, and references therein). In this range all bursts are triggered when He burning at the base of the accreted layer becomes thermally unstable (He ignition). The column depth (or density) at the base of the burning layer when ignition occurs is known as ignition depth, y_{ign} , and the time between bursts is simply $t_{\text{rec}} = y_{\text{ign}}/\dot{m}$.

As H burns at a constant rate (temperature and \dot{m}

independent, but proportional to Z), the time it takes to consume all H in a sinking fluid element depends only on X_0 and Z :

$$t_{\text{burn}} = 27 \text{ hr} \left(\frac{X_0}{0.7} \right) \left(\frac{0.01}{Z} \right) (1+z)/1.31 \quad (2)$$

(as seen by an observer; e.g., Galloway & Cumming 2006), where $1+z=(1-2GM/Rc^2)^{-1/2}=1.31$ is the gravitational redshift on the surface of a NS with mass $M=1.4 M_\odot$ and radius $R=10$ km. The longest burst recurrence time that we measure in T5X2 is $t_{\text{rec}} \sim 1$ hr. For Solar abundances this implies that $t_{\text{rec}} \ll t_{\text{burn}}$, i.e., there is no time to consume all H between the T5X2 bursts unless the fuel is substantially H-poor and/or metal rich (see below). In general, for accretion rates

$$\dot{m} > \dot{m}_{\text{dep}} \simeq 0.04 \dot{m}_{\text{Edd}} \left(\frac{0.7}{X_0} \right) \left(\frac{Z}{0.01} \right)^{13/18} \quad (3)$$

(Bildsten 1998, for $M=1.4 M_\odot$ and $R=10$ km), there is no time to burn the accreted H before reaching ignition conditions (i.e., $t_{\text{rec}} < t_{\text{burn}}$) so that He ignites in a mixture of H and He. In this regime y_{ign} does not depend sensitively on \dot{m} , and a simple $t_{\text{rec}} \propto \dot{m}^{-1}$ relation is expected. For $\dot{m} < \dot{m}_{\text{dep}}$ instead, there is enough time to deplete all H before the base of the accreted layer reaches ignition conditions. Bursts are then triggered in the absence of H (pure He ignition). In this regime y_{ign} decreases with increasing \dot{m} , which results in a steeper decline of the burst recurrence time as \dot{m} increases, close to $t_{\text{rec}} \propto \dot{m}^{-3}$ (Cumming & Bildsten 2000).

This transition between pure He and mixed H/He ignition regimes can be seen in the E_b - \dot{m} and t_{rec} - \dot{m} relations in Figure 11, where we show two semi-analytic models from Cumming & Bildsten (2000) with different compositions. Even though the transition from pure He to mixed H/He ignition is expected at $\dot{m}_{\text{dep}} \sim 0.05 \dot{m}_{\text{Edd}}$ for the case of Solar abundances, Figure 11 and Equation 3 clearly show that changes in the accreted composition can increase \dot{m}_{dep} by a factor of at least 10. In particular, Figure 11 shows that ignition models with low H abundance, $[X_0=0.1, Z=0.02]$, can reproduce the change in slope of both the E_b - L_{pers} and t_{rec} - L_{pers} relations that we observe in T5X2 at $L_{\text{pers}} \simeq 0.3 L_{\text{Edd}}$, i.e., at the transition between regimes B and C (Sec. 3.2, Tables 3 & 4). With such low X_0 , H can be depleted before reaching He ignition at accretion rates much higher than in the case of Solar abundances, which highlights the importance of fuel composition in the burning regimes.

The average T5X2 accretion-to-burst energy ratio ($\alpha=Q_{\text{grav}}(1+z)/Q_{\text{nuc}}$), $\langle \alpha \rangle = 102$, corresponds to a total nuclear energy release during the bursts $Q_{\text{nuc}} \simeq 2.8 \text{ MeV nucleon}^{-1}$ (see also Motta et al. 2011). Taking $Q_{\text{nuc}} = 1.6 + 4\langle X \rangle \text{ MeV nucleon}^{-1}$ (which assumes complete burning of the accumulated fuel and $\sim 35\%$ neutrino energy loss; Galloway et al. 2008, and references therein) we find an average H mass fraction over the burning layer $\langle X \rangle \simeq 0.3$. Such low inferred Q_{nuc} lends support to the low H fraction fuel scenario for T5X2 proposed above. In summary, the slopes of the E_b - L_{pers} and t_{rec} - L_{pers} relations as well as the α values observed during the T5X2 outburst, indicate a low accreted H fraction and strongly suggest a transition from the pure He

ignition regime to the mixed H/He ignition regime happening during the outburst rise when \dot{m} increases above $\sim 0.3 \dot{m}_{\text{Edd}}$. It is worth noting that the reverse transition is observed during the outburst decay when \dot{m} drops below $0.3 \dot{m}_{\text{Edd}}$ (i.e., the outburst rise and decay tracks overlap and no hysteresis is seen in Figures 7 & 8).

We stress that the link between the observed T5X2 *bursting* regimes and the theoretical *burning* regimes that we put forward is based on the t_{rec} - L_{pers} and E_b - L_{pers} relations. Modeling and interpretation of the individual burst light curves is beyond the scope of this work, yet we note that different burst light curves and peak luminosities are predicted in the different ignition regimes (e.g. Woosley et al. 2004). Pure He bursts are expected to show faster rise times than mixed H/He bursts. This agrees qualitatively with the identification of regime B as pure He ignition: t_{rise} is shorter in regime B than in regime C (Fig. 9). The large change in L_{pers} , however, could influence the observed timescales along the burst rise and decay, as these are measured after subtracting the persistent emission. It should also be noted that at low accretion rates (near $\dot{m}_{\text{SHB}} \simeq 0.08 \dot{m}_{\text{Edd}}$ for $X_0=0.1, Z=0.02$) there should be a transition to H-ignited bursts, not included in the models discussed in this Section (Cumming & Bildsten 2000).

If the link between bursting and burning regimes that we propose is correct, to our knowledge this is the first time that the transition between pure He and mixed H/He ignition is observed in a single source. There is, however, a systematic and interesting discrepancy evident in Figure 11. Even when including compressional heating or when increasing the base heat flux from the NS crust (up to $2 \text{ MeV nucleon}^{-1}$; fixed at $0.1 \text{ MeV nucleon}^{-1}$ in Fig. 11; Cumming & Bildsten 2000), ignition models predict higher burst energies and longer recurrence times than those we find in T5X2, by a factor close to 10 in most cases (i.e., larger than the distance uncertainty on L_{pers} and E_b , Sec. 2). This large difference between the observed and predicted values of E_b and t_{rec} , together with the lack of detailed modeling of the T5X2 burst light curves, prevents a conclusive identification of the observed bursting regimes.

We propose that such discrepancy could be explained by the presence of an extra source of heat in the NS envelope not accounted for by ignition models (which typically consider only hot-CNO heating). Additional heat would act to reduce y_{ign} and thereby decrease E_b and t_{rec} , explaining the T5X2 observations presented herein. Several interesting possibilities for the nature of this extra source of heat have been partially investigated, including: i) heating due to stable He burning (triple alpha reaction rates have been recently debated; e.g., Ogata et al. 2009; Dotter & Paxton 2009; Peng & Ott 2010); ii) heating due to deep burning of residual H (e.g., Taam et al. 1996, who already pointed out that it can lead to weaker and more frequent bursts than expected); iii) thermal inertia, “hot ashes” or heat from previous bursts, which could become important for T5X2 as it features $t_{\text{rec}} \sim 200\text{s}$, the shortest recurrence times between thermonuclear bursts ever observed (time-dependent simulations of a series of bursts are needed to investigate this in detail; e.g., Heger et al. 2007b) and iv) turbulent friction at the base of the spreading

layer, which could release substantial amounts of heat (Inogamov & Sunyaev 2010). It is worth noting that an independent study of the same source (Degenaar et al. 2011) reached similar conclusions, suggesting the presence of a “shallow heat source” in T5X2 in order to reconcile quiescent observations and crust heating/cooling theory. Without regard to the exact nature of this heat source, we have shown in the present work that the burst properties of T5X2 place new constraints on the thermal properties of a fast-accreting and frequently-bursting NS.

4.2. mHz QPOs and marginally stable burning

The mHz QPOs from T5X2 (Sec. 3.1; see also Linares et al. 2010a) have distinctive properties that clearly set them apart from the previously known mHz QPOs (Sec. 1; Revnivtsev et al. 2001; Altamirano et al. 2008). The persistent luminosity that we measure in T5X2 when mHz QPOs are present is about 10 times higher than that observed in previous mHz QPO sources (L_{pers} higher by a factor of 4–25 taking into account the observed ranges: 0.02–0.1 L_{Edd} in atoll sources as opposed to 0.4–0.5 L_{Edd} in T5X2; Table 2). For this reason we refer to the previously known mHz QPOs as “low- L_{pers} mHz QPOs”.

Bright bursts and low- L_{pers} mHz QPOs alternate, while remaining clearly distinguishable. Instead, in T5X2 bursts smoothly evolve into mHz QPOs and vice versa (Sec. 3.1), a phenomenon never observed before. Strikingly, the same qualitative evolution from bright infrequent bursts to faint and frequent bursts, mHz QPOs and ultimately stable burning is predicted to happen as \dot{m} increases by both one-zone models and detailed simulations of nuclear burning on NSs accreting near the boundary between unstable and stable He burning (Heger et al. 2007b). We can therefore identify with confidence the mHz QPOs from T5X2 with marginally stable burning on the NS surface. The evidence that links low- L_{pers} mHz QPOs with marginally stable burning is less conclusive, but remains valid (see Revnivtsev et al. 2001; Yu & van der Klis 2002; Altamirano et al. 2008, for details).

Analytic estimates place the threshold for stable He burning at

$$\dot{m}_{\text{sb}} \simeq 1.1 \dot{m}_{\text{Edd}} \left(\frac{1.7}{1 + X_0} \right)^{3/4} \left(\frac{Y_0 \mu}{0.3 \times 0.6} \right)^{1/2}, \quad (4)$$

where μ is the mean molecular weight of the accreted fuel (Bildsten 1998, assuming again $M=1.4 M_{\odot}$ and $R=10$ km).

The persistent luminosity where mHz QPOs are observed in T5X2 (0.4–0.5 L_{Edd}) is therefore closer to the expected value of \dot{m}_{sb} than what was seen in low- L_{pers} mHz QPOs, yet still inconsistent with the value predicted by theory, which is higher by a factor of ~ 2 (unless Terzan 5 is at ~ 9 kpc instead of 6.3 kpc, Sec. 2). Invoking H-poor fuel makes this discrepancy even larger, as it can increase the expected \dot{m}_{sb} by a factor 2 (for $X_0=0.1$, $Z=0.01$; Eq. 4). A more massive NS can have unstable burning at higher \dot{m} than a less massive star, but given the weak ($M^{1/2}$) scaling of \dot{m}_{sb} different NS masses cannot explain the large difference (factor 4–25) in L_{pers} between T5X2 and the other known sources of mHz QPOs. Another remarkable difference between the mHz QPOs

presented herein and the low- L_{pers} mHz QPOs resides in their fractional rms spectrum (Sec. 2): we find a fractional rms amplitude that increases with energy between 2 and 20 keV (Sec. 3.1), while Revnivtsev et al. (2001) reported fractional amplitudes decreasing with increasing photon energy between 2 and 5 keV. The energy-averaged fractional amplitudes are, however, similar (1.3–2.2 % in T5X2, this work; 0.7–1.9 % in low- L_{pers} mHz QPOs, Revnivtsev et al. 2001). The increase of fractional amplitude with energy that we find is shallower than the linear increase predicted by models of temperature oscillations at the NS surface (developed in the context of burst oscillations; Piro & Bildsten 2006).

An interesting possibility is that the low- L_{pers} mHz QPOs trace the boundary of stable H burning (Eq. 1), whereas the mHz QPOs that we discovered in T5X2, at a higher accretion rate, occur at the boundary of stable He burning (Eq. 4). This remains speculative at present given the lack of published theoretical work on this particular topic. A specific analysis of oscillatory burning at the thermal stability boundary of H burning is needed to address this hypothesis. The oscillatory behavior at the marginally stable point is generic (Paczynski 1983) and it could also occur when H burning stabilizes. If low- L_{pers} mHz QPOs do happen at the H burning stability boundary, the need to invoke confined accretion to explain their low L_{pers} would vanish.

Heger et al. (2007b) found that the QPO frequency is mainly sensitive to the accreted H fraction (X_0) and the NS surface gravity: increasing the surface gravity or decreasing X_0 leads to higher mHz QPO frequencies. The highest ν_{QPO} values that we find in T5X2 (4.2 mHz) are about a factor of 3 lower than those of the low- L_{pers} mHz QPOs (Table 2; Revnivtsev et al. 2001; Altamirano et al. 2008). If the accreted fuel has a similar composition, and if the mHz QPOs have the same origin, this would suggest a less compact NS in T5X2 than in the low- L_{pers} mHz QPO sources (the “atoll” sources 4U 1636-536, 4U 1608-52 and Aql X-1). Comparing to models of marginally stable burning, we find that if $X_0 < 0.7$ the surface gravity of the NS in T5X2 must be $g = GM/R^2 < 1.9 \times 10^{14} \text{ cm s}^{-2}$ (Figure 9 in Heger et al. 2007b). Even though it is subject to theoretical (based on analytic one-zone model) and observational (a new outburst of T5X2 could show higher ν_{QPO}) uncertainties, this illustrates how a comparison between marginally stable burning models and mHz QPO properties can be used to constrain the NS compactness.

Despite the striking similarities between the T5X2 burst properties and the general bursting behavior predicted by models of nuclear burning near the transition from unstable to stable burning (cf. Fig. 1 in this work and Fig. 5 in Heger et al. 2007b), interesting differences remain. First, as explained above, the \dot{m} where marginally stable burning is expected (0.925 \dot{m}_{Edd} Heger et al. 2007b) is higher than the highest inferred \dot{m} where we observe mHz QPOs in T5X2 (0.5 \dot{m}_{Edd}). Second, Heger et al. (2007b) find a sharp transition from bursts to mHz QPOs and finally stable burning (occurring between 0.923–0.95 \dot{m}_{Edd}), while we observe in T5X2 a smooth evolution from bursts to mHz QPOs, and vice versa (between 0.1–0.5 \dot{m}_{Edd} ; Sec. 3). Time-dependent simulations of nuclear burning tailored to T5X2 would be of high interest, in particular exploring

the H-poor fuel range. Third, we find that the disappearance of the mHz QPOs in T5X2 is not linked to an increase in \dot{m} but to an actual *drop* of L_{pers} that happens when the accretion state changes (from horizontal to normal & flaring branches). This suggests that the geometry/configuration of the accretion flow plays a role in setting the nuclear burning stability boundary.

4.3. The role of an intermediate magnetic field

While most models of thermonuclear bursts on accreting NSs assume that the NS magnetic field is negligible (Fujimoto et al. 1981; Taam 1982; Paczynski 1983; Woosley et al. 2004), Joss & Li (1980) showed that the presence of a strong ($B \gtrsim 10^{12}$ G) magnetic field can affect the stability of nuclear burning in different ways. A strong magnetic field reduces the (conductive and radiative) opacities, allowing for more efficient heat transport and thereby stabilizing burning. Applying disk-magnetosphere interaction models to T5X2, Papitto et al. (2011) estimated $B = 2 \times 10^8 - 2.4 \times 10^{10}$ G from the luminosity range at which pulsations were detected, whereas Miller et al. (2011) further constrained $B = (0.7 - 4) \times 10^9$ G from the Fe line profile. The fact that T5X2 shows thermonuclear bursts suggests that the magnetic field needed to suppress the thermal instability and quench thermonuclear bursts must be greater than $\sim 10^{10}$ G, in accordance with theoretical expectations (Joss & Li 1980).

A strong magnetic field also affects convective heat transport and mixing (e.g. Joss & Li 1980). Bildsten (1995) proposed that even in cases where thermonuclear burning is unstable the presence of a strong magnetic field can suppress convection in the NS envelope, stalling the propagation of the burning front (diffusive heat transport being slower than convection) and preventing the fast ignition that causes type I X-ray bursts (see also Bildsten 1998). Again, the mere presence of type I X-ray bursts in T5X2 strongly suggests that the magnetic field required to suppress convective burning fronts must be higher than $\sim 10^{10}$ G, in agreement with analytical estimates (Joss & Li 1980; Bildsten & Brown 1997). Rise times are rather long though (Fig. 9), which could perhaps indicate that B is strong enough to slow down the burning fronts (Bildsten & Brown 1997). In summary, the bursting properties of T5X2 presented herein (in particular combined with refined measurements of its magnetic field strength) can place new constraints on the physics of convection and heat transport under intermediate magnetic fields ($10^8 - 10^{10}$ G).

Finally, a $10^8 - 10^{10}$ G magnetic field can also channel the accretion flow onto the magnetic polar caps, as suggested by theoretical models of disk-magnetosphere interaction (Lamb et al. 1973) and by the presence of X-ray pulsations in T5X2 (Strohmayer & Markwardt 2010; Papitto et al. 2011). Accretion confined to the magnetic polar caps may break the spherical symmetry assumed by most thermonuclear burst models, and increase \dot{m} for a given (observed) L_{pers} (Sec. 2). The impact on the burning properties depends on the size of the polar caps and on how soon the accreted fuel spreads laterally while sinking into the NS envelope under the influence of a magnetic field. Bildsten & Brown (1997) found that for dipolar magnetic fields $B < (2 - 4) \times 10^{10}$ G, the accreted

fuel spreads before igniting and the spherically symmetric case is recovered. This suggests that the T5X2 burst properties can still be compared to spherically symmetric ignition models (Sec. 4.1).

As the size and “depth” of the polar caps are nevertheless ill-constrained quantities, we explore a simple scenario in which the fuel in T5X2 is confined into a 10% of the NS surface down to ignition depth, y_{ign} . From geometrical considerations, assuming the same y_{ign} predicted by ignition models (Cumming & Bildsten 2000), in this confined scenario bursts would be 10 times less energetic and 10 times more frequent than in the spherically symmetric case, which would explain the mismatch between predicted and observed E_b and t_{rec} (Sec. 4.1). However, the accretion rate per unit area would also increase by a factor 10, which for the observed L_{pers} implies that unstable burning would operate at \dot{m} as high as ~ 5 times \dot{m}_{Edd} . This is well above the predicted threshold for stable steady burning of H and He (\dot{m}_{sb} , Eq. 4; see also Bildsten 1998), and we therefore consider this scenario unlikely. If the accreted material contains no H, however, \dot{m}_{sb} can be several times larger than \dot{m}_{Edd} (Bildsten 1998).

4.4. Rotation, mixing and burning

The unique bursting behavior in T5X2 is, in essence, much closer to what theory predicts than any other burster known to date. Theoretical burning regimes were mostly based on models that assume a non-rotating NS and radial infall of the accreted mass (Fujimoto et al. 1981; Bildsten 1998). These are admittedly simplistic assumptions, as NSs in LMXBs can have spin frequencies in excess of 600 Hz and the orbital frequencies in the innermost accretion disk are well above 1000 Hz. The accretion of matter with angular momentum onto a spinning NS introduces a shear in its surface layers (Piro & Bildsten 2007; Keek et al. 2009, and references therein). The main effect of rotation which may have an impact on burning regimes is turbulent mixing. In particular, Keek et al. (2009) found that such rotationally induced turbulent mixing stabilizes He burning, decreasing the burning stability boundary (\dot{m}_{sb}).

Motivated by the stronger magnetic field (factor ~ 10) and slower spin (factor $\gtrsim 20$) of T5X2 compared to the rest of bursters, we speculate that rotationally induced turbulent mixing is what sets T5X2 apart from the rest of thermonuclear burst sources. The stronger B field could channel a large fraction of the accreted matter into the NS magnetic poles and produce a more radial inflow which would then spread over the whole surface, minimizing shear and turbulent mixing. Therefore T5X2 seems to meet to a greater extent the assumptions of zero spin and radial infall mentioned above, which can explain the better agreement with theory. This in turn suggests that, as argued by Piro & Bildsten (2007) and Keek et al. (2009), the effects of rotation must be considered to explain the behavior of most bursters.

5. SUMMARY AND CONCLUSIONS

We have presented the discovery of mHz QPOs from the NS-LMXB and 11 Hz X-ray pulsar T5X2, as well as the full bursting properties during its 2010 outburst, when the persistent luminosity varied by about a factor

of 5 (between $L_{\text{pers}} \simeq 0.1\text{--}0.5 L_{\text{Edd}}$). T5X2 showed copious thermonuclear bursts when $L_{\text{pers}} \gtrsim 0.2 L_{\text{Edd}}$, a regime where thermonuclear bursts had proven exceptional to date. Burst energies and recurrence times gradually decreased as L_{pers} increased, turning into a rapid series of faint bursts and smoothly evolving into a mHz QPO near the outburst peak. Only at the highest L_{pers} range bursts became undetectable during a few short intervals. This behavior is both unprecedented among bursters and remarkably similar to the nuclear burning regimes expected on an accreting NS near the boundary of stable He burning.

We find four different bursting regimes when studying the relation between burst properties and L_{pers} and show that in one of such regimes the burst recurrence time decays steeply with increasing L_{pers} , close to $t_{\text{rec}} \propto L_{\text{pers}}^{-3}$. By confronting the change in burst properties (in particular, the relation between E_b , t_{rec} and L_{pers}) to ignition model predictions, we find evidence of a transition between pure He and mixed H/He ignition occurring in T5X2 when $L_{\text{pers}} \simeq 0.3 L_{\text{Edd}}$. We note that large discrepancies remain between the observed T5X2 burst proper-

ties and those predicted by theory at high mass accretion rates. We further argue that the accreted fuel is H-poor and suggest that an additional source of heat in the NS envelope is needed to reconcile the observed and predicted burst properties.

We examine the properties of the mHz QPOs from T5X2 in the context of marginally stable burning models, and compare them to those of previously known mHz QPO sources. T5X2 features mHz QPOs with lower frequencies (by a factor ~ 3), when L_{pers} is substantially higher (by a factor $\sim 4\text{--}25$). Finally, we discuss the role of magnetic field and spin in setting the unique T5X2 burst and mHz QPO behavior, and speculate that the absence of rotation effects such as turbulent mixing of the accreted fuel may set T5X2 apart from the rest of bursters.

We thank M. van der Klis for detailed comments on the manuscript. We are grateful to the International Space Science Institute in Bern, where part of this work was completed. ML acknowledges support from the NWO Rubicon fellowship.

REFERENCES

- Altamirano, D., van der Klis, M., Wijnands, R., & Cumming, A. 2008, *ApJ*, 673, L35
- Altamirano, D., Watts, A., Linares, M., Markwardt, C. B., Strohmayer, T., & Patruno, A. 2010a, *MNRAS*, 409, 1136
- Altamirano, D., et al. 2010b, *The Astronomer's Telegram*, 2932, 1
- . 2010c, *The Astronomer's Telegram*, 2952, 1
- Belian, R. D., Conner, J. P., & Evans, W. D. 1976, *ApJ*, 206, L135
- Bildsten, L. 1995, *ApJ*, 438, 852
- Bildsten, L. 1998, in *NATO ASIC Proc. 515: The Many Faces of Neutron Stars.*, ed. R. Buccheri, J. van Paradijs, & A. Alpar, 419–+
- Bildsten, L. 2000, in *American Institute of Physics Conference Series*, Vol. 522, American Institute of Physics Conference Series, ed. S. S. Holt & W. W. Zhang, 359–369
- Bildsten, L., & Brown, E. F. 1997, *ApJ*, 477, 897
- Bildsten, L., et al. 1997, *ApJS*, 113, 367
- Bordas, P., et al. 2010, *The Astronomer's Telegram*, 2919, 1
- Caballero, I., & Wilms, J. 2011, *MemSAIt*, submitted, 0
- Cavecchi, Y., et al. 2011, *ApJ*, 740, L8+
- Chakrabarty, D., Morgan, E. H., Muno, M. P., Galloway, D. K., Wijnands, R., van der Klis, M., & Markwardt, C. B. 2003, *Nature*, 424, 42
- Chakrabarty, D., & Roche, P. 1997, *ApJ*, 489, 254
- Chakrabarty, M., & Bhattacharyya, S. 2011, *ApJ*, 730, L23+
- Chenevez, J., et al. 2010, *The Astronomer's Telegram*, 2924, 1
- Cohn, H. N., Lugger, P. M., Grindlay, J. E., & Edmonds, P. D. 2002, *ApJ*, 571, 818
- Cornelisse, R., et al. 2003, *A&A*, 405, 1033
- Cui, W. 1997, *ApJ*, 482, L163+
- Cumming, A., & Bildsten, L. 2000, *ApJ*, 544, 453
- dal Fiume, D., et al. 1998, *A&A*, 329, L41
- Degenaar, N., Brown, E. F., & Wijnands, R. 2011, *ArXiv e-prints* 1107.5317; submitted to *MNRAS*
- Dotter, A., & Paxton, B. 2009, *A&A*, 507, 1617
- Falanga, M., et al. 2011, *A&A*, 529, A68+
- Finger, M. H., Koh, D. T., Nelson, R. W., Prince, T. A., Vaughan, B. A., & Wilson, R. B. 1996, *Nature*, 381, 291
- Fujimoto, M. Y., Hanawa, T., & Miyaji, S. 1981, *ApJ*, 247, 267
- Galloway, D. K., & Cumming, A. 2006, *ApJ*, 652, 559
- Galloway, D. K., Cumming, A., Kuulkers, E., Bildsten, L., Chakrabarty, D., & Rothschild, R. E. 2004, *ApJ*, 601, 466
- Galloway, D. K., & in't Zand, J. J. M. 2010, *The Astronomer's Telegram*, 3000, 1
- Galloway, D. K., Muno, M. P., Hartman, J. M., Psaltis, D., & Chakrabarty, D. 2008, *ApJS*, 179, 360
- Grindlay, J., Gursky, H., Schnopper, H., Parsignault, D. R., Heise, J., Brinkman, A. C., & Schrijver, J. 1976, *ApJ*, 205, L127
- Hasinger, G., & van der Klis, M. 1989, *A&A*, 225, 79
- Heger, A., Cumming, A., Galloway, D. K., & Woosley, S. E. 2007a, *ApJ*, 671, L141
- Heger, A., Cumming, A., & Woosley, S. E. 2007b, *ApJ*, 665, 1311
- Heinke, C. O., Wijnands, R., Cohn, H. N., Lugger, P. M., Grindlay, J. E., Pooley, D., & Lewin, W. H. G. 2006, *ApJ*, 651, 1098
- Hinkle, K. H., Fekel, F. C., Joyce, R. R., Wood, P. R., Smith, V. V., & Lebzelter, T. 2006, *ApJ*, 641, 479
- Hoffman, J. A., Marshall, H. L., & Lewin, W. H. G. 1978, *Nature*, 271, 630
- Inogamov, N. A., & Sunyaev, R. A. 2010, *Astronomy Letters*, 36, 848
- Jonker, P. G., & van der Klis, M. 2001, *ApJ*, 553, L43
- Joss, P. C., & Li, F. K. 1980, *ApJ*, 238, 287
- Keek, L., Galloway, D. K., in't Zand, J. J. M., & Heger, A. 2010, *ApJ*, 718, 292
- Keek, L., & in't Zand, J. J. M. 2008, in *Proceedings of the 7th INTEGRAL Workshop*
- Keek, L., Langer, N., & in't Zand, J. J. M. 2009, *A&A*, 502, 871
- Kouveliotou, C., van Paradijs, J., Fishman, G. J., Briggs, M. S., Komers, J., Harmon, B. A., Meegan, C. A., & Lewin, W. H. G. 1996, *Nature*, 379, 799
- Lamb, F. K., Pethick, C. J., & Pines, D. 1973, *ApJ*, 184, 271
- Lanzoni, B., et al. 2010, *ApJ*, 717, 653
- Lewin, W. H. G., & Joss, P. C. 1977, *Nature*, 270, 211
- Lewin, W. H. G., van Paradijs, J., & Taam, R. E. 1993, *Space Science Reviews*, 62, 223
- Linares, M., Chakrabarty, D., & van der Klis, M. 2011, *ApJ*, 733, L17+
- Linares, M., et al. 2009, *The Astronomer's Telegram*, 1979, 1
- . 2010a, *The Astronomer's Telegram*, 2958, 1
- . 2010b, *ApJ*, 719, L84
- Lomb, N. R. 1976, *Ap&SS*, 39, 447
- Maraschi, L., & Cavaliere, A. 1977, in *X-ray Binaries and Compact Objects*, ed. K. A. van der Hucht, 127–128
- Markwardt, C. B., Altamirano, D., Swank, J. H., Strohmayer, T. E., Linares, M., & Pereira, D. 2009, *The Astronomer's Telegram*, 2197, 1
- Mihara, T., Makishima, K., Ohashi, T., Sakao, T., & Tashiro, M. 1990, *Nature*, 346, 250
- Miller, J. M., Maitra, D., Cackett, E. M., Bhattacharyya, S., & Strohmayer, T. E. 2011, *ApJ*, 731, L7
- Motta, S., D'Ai, A., Papitto, A., Riggio, A., Di Salvo, T., Burderi, L., Stella, T. B. L., & Iaria, R. 2011, *MNRAS*, 414, 1508

- Ogata, K., Kan, M., & Kamimura, M. 2009, *Progress of Theoretical Physics*, 122, 1055
- Orlandini, M., et al. 1998, *ApJ*, 500, L163+
- Ortolani, S., Barbuy, B., Bica, E., Zoccali, M., & Renzini, A. 2007, *A&A*, 470, 1043
- Paczynski, B. 1983, *ApJ*, 264, 282
- Papitto, A., D’Ai, A., Motta, S., Riggio, A., Burderi, L., di Salvo, T., Belloni, T., & Iaria, R. 2011, *A&A*, 526, L3+
- Patruno, A. 2010, *ApJ*, 722, 909
- Peng, F., & Ott, C. D. 2010, *ApJ*, 725, 309
- Piro, A. L., & Bildsten, L. 2006, *ApJ*, 638, 968
- . 2007, *ApJ*, 663, 1252
- Pooley, D., Homan, J., Heinke, C., Linares, M., Altamirano, D., & Lewin, W. 2010, *The Astronomer’s Telegram*, 2974, 1
- Psaltis, D., & Chakrabarty, D. 1999, *ApJ*, 521, 332
- Rappaport, S., Markert, T., Li, F. K., Clark, G. W., Jernigan, J. G., & McClintock, J. E. 1977, *ApJ*, 217, L29
- Revnivtsev, M., Churazov, E., Gilfanov, M., & Sunyaev, R. 2001, *A&A*, 372, 138
- Scargle, J. D. 1982, *ApJ*, 263, 835
- Strohmayer, T. E., & Markwardt, C. B. 2010, *The Astronomer’s Telegram*, 2929, 1
- Strohmayer, T. E., Markwardt, C. B., Pereira, D., & Smith, E. A. 2010, *The Astronomer’s Telegram*, 2946, 1
- Strohmayer, T. E., & Smith, E. A. 2011, *The Astronomer’s Telegram*, 3258, 1
- Sturmer, S. J., & Dermer, C. D. 1996, *ApJ*, 465, L31+
- Taam, R. E. 1981, *Ap&SS*, 77, 257
- . 1982, *ApJ*, 258, 761
- Taam, R. E., Woosley, S. E., & Lamb, D. Q. 1996, *ApJ*, 459, 271
- Tanaka, Y. 1989, in *ESA Special Publication*, Vol. 296, *Two Topics in X-Ray Astronomy, Volume 1: X Ray Binaries*.
- Volume 2: AGN and the X Ray Background, ed. J. Hunt & B. Battrick, 3–13
- Truemper, J., Pietsch, W., Reppin, C., Voges, W., Staubert, R., & Kendziorra, E. 1978, *ApJ*, 219, L105
- Ubertini, P., Bazzano, A., Cocchi, M., Natalucci, L., Heise, J., Muller, J. M., & in ’t Zand, J. J. M. 1999, *ApJ*, 514, L27
- van Paradijs, J., Penninx, W., & Lewin, W. H. G. 1988, *MNRAS*, 233, 437
- Woosley, S. E., & Taam, R. E. 1976, *Nature*, 263, 101
- Woosley, S. E., et al. 2004, *ApJS*, 151, 75
- Yu, W., & van der Klis, M. 2002, *ApJ*, 567, L67